Characteristics of fast timing MCP-PMTs in magnetic fields

Mohammad Hattawy[a,b], Junqi Xie[a,*], Mickey Chiu[c], Marcel Demarteau[a], Kawtar Hafidi[a], Edward May[a], Jose Repond[a], Robert Wagner[a], Lei Xia[a], Carl Zorn[d]

[a] *Argonne National Laboratory, 9700 S. Cass Ave., Argonne, IL 60439, USA*
[b] *Old Dominion University, 5115 Hampton Blvd., Norfolk, VA 23529, USA*
[c] *Brookhaven National Laboratory, 2 Center St., Upton, NY 11973, USA*
[d] *Thomas Jefferson National Accelerator Facility, 12000 Jefferson Ave., Newport News, VA 23606, USA*

Abstract

Performance of the microchannel plate photomultiplier tube (MCP-PMT) in magnetic fields is an essential aspect for its application in the proposed electron ion collider. The motivation of this paper is to explore the critical parameters that affect the performance of MCP-PMT in magnetic fields and to guide the design optimization of MCP-PMTs for high magnetic field tolerance. MCP-PMTs with two different designs were examined in magnetic fields, and the results were compared. The magnetic field tolerance of MCP-PMT with new independently biased voltage design shows significant improvement (up to 0.7 T) compared to that of the MCP-PMT with resistor chain design (up to 0.1 T), indicating that optimization of the individual MCP voltage is an essential parameter for magnetic field tolerance improvement. The effects of other parameters such as the rotation angle relative to the magnetic field direction and the bias voltage between the photocathode and entrance MCP were thoroughly studied with the independently biased voltage design. The signal amplitude of the MCP-PMT exhibits enhanced performance at $\pm 8^\circ$ tilt angle due to the original MCP 8° bias angle. Maximum signal amplitude values are observed depending on the optimal bias voltages in different magnetic field strength.

Keywords: Fast timing, Microchannel plate, Photodetector, Electron Ion Collider, Particle identification detector, Rate capability, Magnetic field, Rotation angle.

1. Introduction

The Electron-Ion Collider (EIC) [1], which is recommended in the 2015 Long Range Plan for Nuclear Science [2] as the highest priority for a new facility construction in the US, aims to revolutionize our understanding both of nucleon and nuclear structure and of nuclear dynamics in the many-body regime, where strongly coupled relativistic quantum fluctuations and non-perturbative effects combine to give dynamic origin to nuclear mass and spin. The broad physics program of EIC requires a large multipurpose spectrometer to measure various physics processes over a wide range of rapidity and solid angle. Among these measurements, particle identification, i.e., the separation of electrons, pions, kaons, and protons (e/π/K/p) in the final state is a fundamental requirement for important physics processes such as semi-inclusive deep inelastic scattering and charm production.

To address the detector requirements for the broad physics program of EIC, several new detector concepts are currently being proposed, including the BeAST detector [3] and sPHENIX detector based on BaBAR solenoid [4] from Brookhaven National Laboratory (BNL), the JLEIC full acceptance detector [5] from Thomas Jefferson National Accelerator Facility (JLab), and the TOPSiDE 5D particle flow detector [6] from Argonne National Laboratory (ANL). These proposed EIC detector concepts have different layouts of sub-systems, some of which have been worked out in detail, and some of which are still placeholders. Nevertheless, all these detector concepts are based on time-of-flight (TOF) systems and imaging Cherenkov detectors for hadron particle identification. Integration of these sub-systems in the central detector involves placing their photo-sensors in the non-uniform fringe field of a solenoidal magnet, requiring low-cost photon sensors with picosecond timing resolution, millimeter spatial resolution, high rate capability, high radiation and magnetic field tolerance.

The microchannel plate photomultiplier tube (MCP-PMT) [7] is a compact photosensor consisting of a photocathode for photon-electron conversion, two MCPs in a stacked chevron configuration for electron amplification and a readout system for charge collection. The compact design and confined electron amplification by secondary electron emission inside the micron size MCP pores provide the MCP-PMT with picosecond timing resolution and millimeter position resolution, ideal for time-of-flight systems and imaging Cherenkov detectors. The LAPPD collaboration [8] between universities, U.S. national laboratories, and industrial partners have developed the technology to manufacture the worlds largest MCP based photosensor, the Large-Area Picosecond Photon Detector (LAPPD^{TM}). A critical aspect of LAPPD^{TM} technology is its use of low-cost, very large area MCPs [9] at 20 cm $\times$ 20 cm size and all glass vacuum envelope. The MCPs for LAPPD^{TM} are made from bundled and fused capillaries of borosilicate

*Corresponding author: jxie@anl.gov (J. Xie)

glass and then functionalized through atomic-layer deposition [10–12] of conductive and secondary-electron emissive material layers. This revolutionary process eliminates the chemical etching and hydrogen firing steps, which are the causes of brittle glass and strong ion feedback in traditional MCP manufacturing. These features and the inherent mechanical stability of borosilicate glass allows the production of the unprecedented large area MCPs with long lifetime [13] and low background noise rates [14].

As a collaborator of the LAPPD project, a dedicated fabrication facility [15] which can produce 6×6 cm^2 MCP-PMTs with the LAPPD design was built at Argonne National Laboratory, serving as a production facility to provide 6×6 cm^2 MCP-PMTs for early users before LAPPD^{TM} are mass produced by our industrial partner, Incom, Inc [16]. Tens of 6×6 cm^2 MCP-PMTs were produced and tested at Argonne and delivered to early users for LAPPD^{TM} feasibility test in their experiments. As Incom, Inc. starts the mass production of the LAPPD^{TM}, the Argonne fabrication facility is converted into an R&D platform for LAPPD^{TM} design optimization for specific applications. Small size (6×6 cm^2) MCP-PMTs with different designs can be quickly produced in the Argonne fabrication facility and tested, and the optimal design can be directly transferred to Incom, Inc. for LAPPD^{TM} mass production.

In this paper, two 6×6 cm^2 MCP-PMTs with different designs were produced in Argonne fabrication facility, and their characteristics in the magnetic field were tested. We describe the different designs of the two MCP-PMTs in details in section 2, the magnetic field tolerance measurement setup in section 3. The experimental results are presented and discussed in section 4, and the conclusions are drawn at the end of this paper.

2. Design of the MCP photodetector

Two MCP-PMTs with different designs were tested in this study: the internal resistor chain design and the independently biased design. The former relies on ALD coated MCPs and spacers inside the MCP-PMT for bias voltage distribution, while the latter relies on external high voltage divider for bias voltage distribution.

2.1. Internal resistor chain MCP-PMT design

The internal resistor chain MCP-PMT design is adapted from the original LAPPD^{TM} design [17]. The left panel of Fig. 1 shows the schematic of the internal resistor chain MCP-PMT design. The sealed vacuum package consists of a photocathode, two MCPs, three grid spacers and a stripline anode. An air-sensitive alkali antimonide photocathode is deposited on the inside surface of the top glass window, and the electronic connection is led out via a pre-coated nichrome layer at the edges of the top window to apply high voltage. Two MCPs with 8o bias angles are placed in chevron geometry to prevent drift of positive ions to the photocathode and to ensure a well-defined first strike of the incoming photoelectrons. The MCPs used here are sliced from the same ALD coated 20 cm × 20 cm MCPs for LAPPD^{TM}, featuring a pore size of 20 μm, a length to diameter (L/d) ratio of 60:1 and an open area ratio of 65%. Glass spacers are used between the photocathode and the top MCP, between the MCPs, and between the bottom MCP and the anode to separate individual components and support the stack configuration. The stripline anode is made by silk-screening of the silver strips onto glass tile base, and each stripline is grounded through a resistor. Here it is vital to note that the MCPs and glass spacers are all coated with resistive materials via ALD method, making the whole detector stack an internal resistor chain, expressed by the dashed line circuit in Fig. 1. When a single high voltage (HV) is applied to the photocathode, the applied HV is distributed between the internal components, controlled by the resistances of the ALD coated MCPs and glass spacers. Signals generated from incident photons are picked up from the stripline anodes and then brought to an oscilloscope or an electronic waveform digitizer.

The internal resistor chain design only requires one HV connection from the inside vacuum envelope to outside through the pre-coated nichrome mask on the top window. This simple design provides the advantages of ease of implementation and potentially low cost. However, processing and testing of the fabricated MCP-PMTs reveal several disadvantages: (a) the HV distribution relies on resistance ratios between the spacers and MCPs, while it is difficult to find precisely matched resistances for the MCPs and spacers; (b) the fabrication of MCP-PMT requires thorough baking and scrubbing of the MCPs under vacuum for outgassing, while experiment processing shows that the resistances of ALD coated MCPs and spacers reduces irregularly during baking and scrubbing process, making the resistance match of MCPs and spacers more diffcult; (c) once the detector is sealed, there is no way to individually optimize the MCPs performance as the bias voltage on each MCP cannot be adjusted separately; (d) the absolute quantum efficiency (QE) of the photocathode cannot be measured using the tradition method as the photocurrent (nA level) generated from incident photons submerges into the continuous bias current (μA level) of the resistor chain.

2.2. Independently biased MCP-PMT design

Due to the irregular reduction of ALD coated MCP and spacer resistances during the photodetector fabrication process, performance of the two MCPs cannot be optimized at the same time. It is necessary to have a new design such that the bias voltage of each MCP can be adjusted independently, referred to as independently biased MCP-PMT design (IBD), so that the performance of both MCPs can be optimized. Schematic of the new IBD design is shown in the right panel of Fig. 1. The major configuration improvement includes: (1) the spacers are bare glass grids with no ALD coating on the surface, so the spacers can be treated as insulators; (2) ultra-thin stainless steel

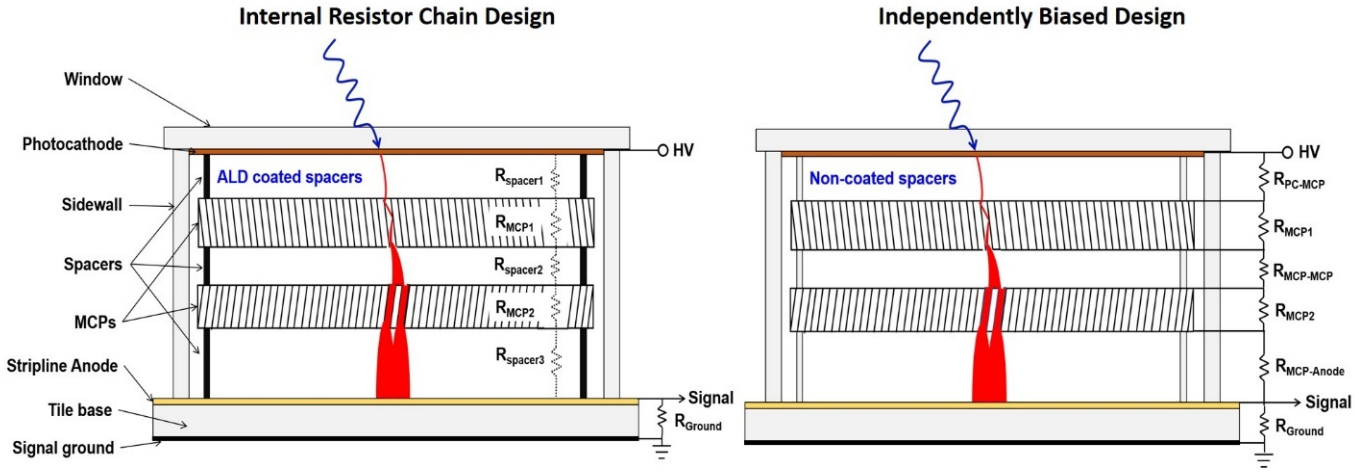

Figure 1: Schematic diagrams of the internal resistor chain design (left) and independently biased design (right). The equivalent electrical circuit in internal resistor chain design is noted as dashed line connections. Notice the major difference of using ALD coated spacers (resistor) in internal resistor chain design and non-coated spacers (insulator) in independently biased design.

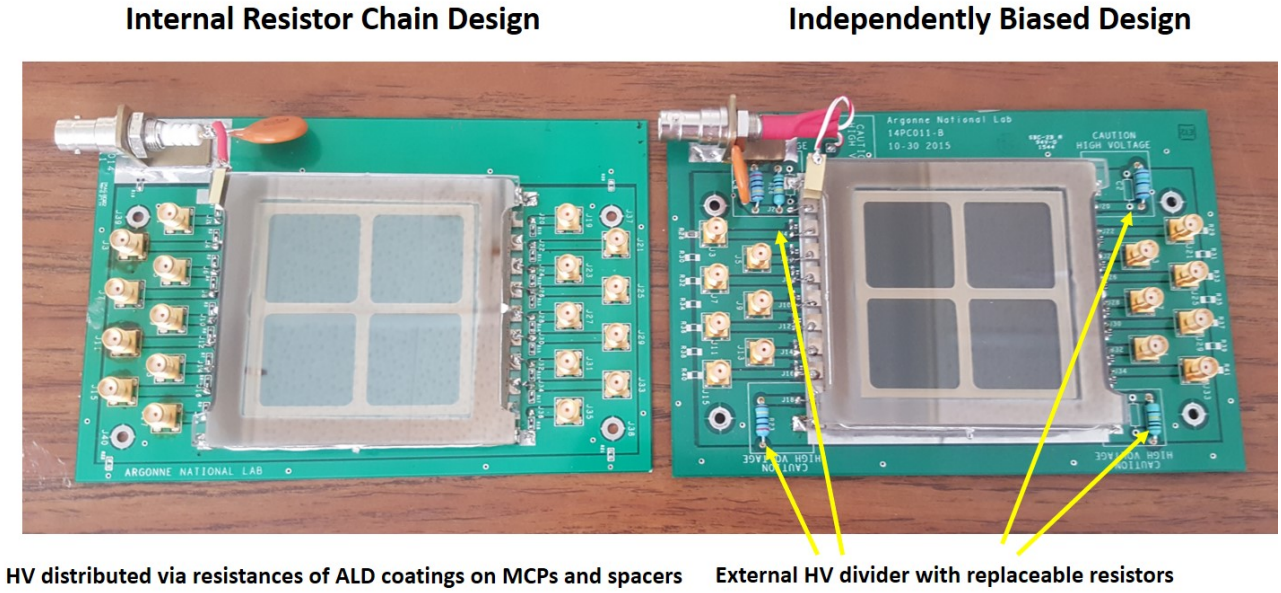

Figure 2: Picture of MCP-PMTs with the internal resistor chain design (left) and independently biased design (right). Simple readout circuit boards were designed to hold the MCP-PMTs. Note that an external HV divider with replaceable resistors was integrated into the readout board of the independently biased MCP-PMT design.

shims with the same pattern as grid spacers are attached between the spacers and the MCP surfaces for HV connections; (3) finger tabs are designed on each shim, leading the shim to the nearest silkscreen printed silver strip contact at the corner, and this leads the MCP surface HV connection to the outside. Four shims are applied for the upper and lower surfaces of the two MCPs. The new IBD design is based on a minimal modification of the internal resistor chain design, using shims and corner strip lines for HV connection, no pins are required to provide high voltage on the MCPs and in the gaps. Fig. 2 shows the picture of a sealed MCP-PMT with the independently biased design (right) in comparison with the internal resistor chain design (left). Simple readout circuit boards were designed to hold the MCP-PMTs. An external resistor chain HV divider is integrated into the readout board of the independently biased MCP-PMT design so that only one HV power supplier is necessary, and the bias voltage of individual MCPs can be independently adjusted by replacing the corresponding resistors.

3. Magnetic field tolerance test facility

At Argonne National Laboratory, a decommissioned superconducting magnet from a magnetic resonance imaging (MRI) scanner was acquired for precise instrument calibration for the g-2 muon experiment [18]. The MRI magnet provides a large bore with a diameter of 68 cm and a very homogeneous field (7 ppb/cm), with a tunable magnetic field strength up to 4 Tesla. This unique facility provides us with a large uniform tunable magnetic field for magnetic field tolerance test of various size detectors. We have built a characterization system compatible with the solenoid magnet to test the performance of the 6×6 cm^2 MCP-PMTs in a strong magnetic field environment. A non-magnetic, light-tight dark box was designed and custom built at the Argonne mechanical shop as a container to constrain the MCP-PMT during the testing within the magnetic field. The dark box was held on a test platform with the detector surface normal to the direction of the magnetic field. The position of the dark box was adjusted so that the center of the MCP photodetector was well-aligned with the center of the solenoid magnet. A rotation mechanism was also integrated with the system, allowing rotation of the MCP-PMTs with an angle θ ($-90° \leq \theta \leq 90°$) during the experiment to study the angle dependence of MCP-PMT performance, as shown in Fig. 3.

Fig. 4 shows a picture of the magnetic field tolerance testing system. A 405 nm light-emitting diode (LED) driven by a pulse generator was used as the light source and was introduced into the dark box through a multimode optical fiber. High voltage was applied to the MCP-PMT from a power supply with continuous voltage control. Signals collected at the striplines were read out through a DT5742 desktop digitizer [19] produced by CAEN (Costruzioni Apparecchiature Elettroniche Nucleari S.p.A.) with a sampling rate of 5 GS/s. The digitizer is based on a switched capacitor array of DRS4 (Domino Ring Sampler) chips [20], 16 analog input channels, and one additional analog input for the fast trigger.

Another MRI magnet with tunable magnetic field up to 3 Tesla was available at the University of Virginia. A similar magnetic field platform without the rotation mechanism was also set up there for part of the experiment. The following results reported in section 4 was completed with either of the two MRI magnets. Specifically, measurement of MCP-PMT with internal resistor chain design was performed on the University of Virginia MRI magnet, and measurement of MCP-PMT with the independently biased design was performed on the Argonne 4-Telsa magnet facility.

4. Results and discussion

The operational principle of MCP-PMTs relies on an electron multiplication process where the channel wall is bombarded multiple times with secondary electrons. Each channel of the MCP used in this experiment has an internal diameter of 20 μm with the inner wall processed with resistive and secondary emissive coating layers, which acts as an independent electron multiplier. When the MCP-PMT is operated in a magnetic field, the trajectories of electrons during electron multiplication process will be affected by the Lorentz force due to the presence of electromagnetic fields. We studied the MCP-PMT performance dependence on magnetic field strength, angle and photocathode to MCP electric field strength as below.

4.1. Magnetic field strength dependence

The performance of MCP-PMTs with the above two designs in the magnetic field was tested at a zero rotation angle θ, i.e., where the direction of the magnetic field is normal to the surface of the MCP photodetector. Since a 405 nm pulsed LED was used here as the light source, the measurements were conducted at a fixed light intensity of 10 photoelectron mode for easy experiment control. The signal amplitude was selected as a relative indicator of the gain and the merit of the MCP-PMT performance in the magnetic field. The results were plotted in terms of the signal amplitude on magnetic field strength as shown in Fig. 5.

The MCP-PMT with internal resistor chain design shows a very poor magnetic field tolerance, the intensity of the peak drops by a factor of 6 with magnetic field increases from 0 to 0.1 Tesla, and another factor of 6 with the magnetic field increases to 0.2 Tesla. This fast drop is mainly because the resistances of the MCPs and spacers were significantly changed during the baking and scrubbing process, resulting in the bias voltage mismatch of the two MCPs. Only one MCP might be biased at the designed optimal HV (typically 1000V per MCP), and the other one

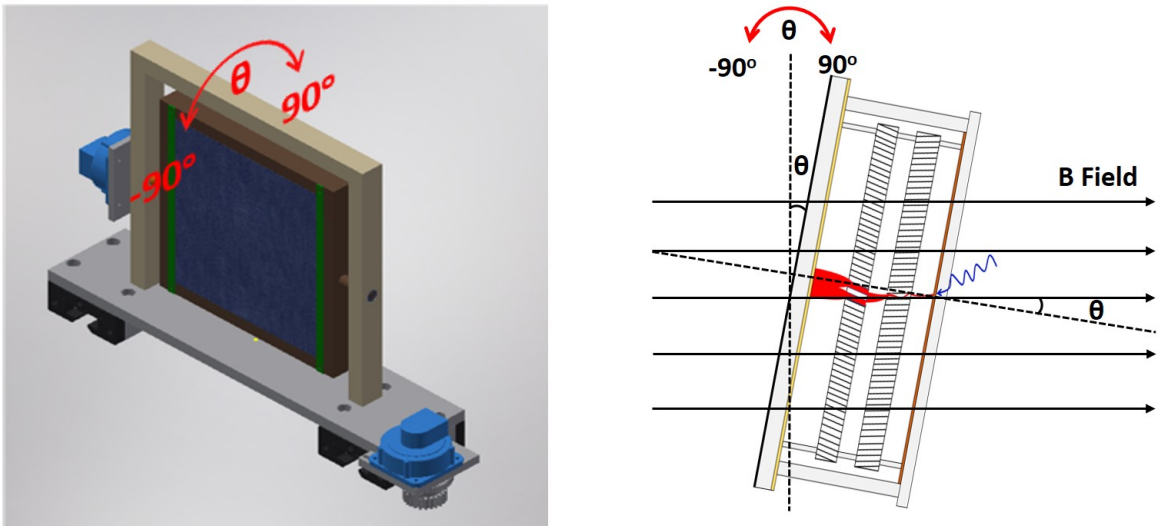

Figure 3: (left) AutoCAD drawing of the custom designed magnetic field tolerance test platform, the center part is rotatable with angle -90° $\leq \theta \leq$ 90°. (right) Schematic of the rotation mechanism of the MCP-PMT with the angle θ relative to the magnetic field direction during the measurement.

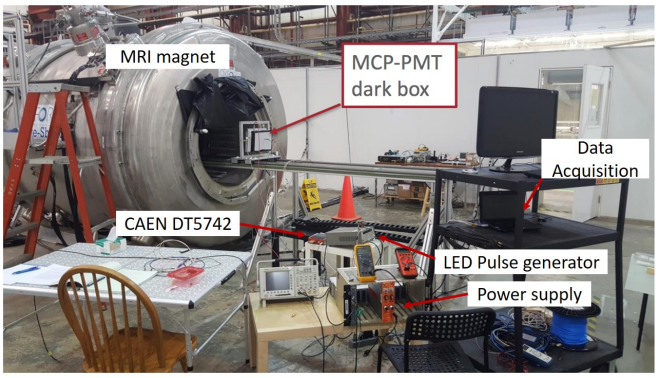

Figure 4: Picture of the magnetic field tolerance testing system.

was biased at HV way off the optimal value. The fast drop of the signal amplitude in the magnetic field indicates that the MCP-PMT with resistor chain design is not suitable for applications in high magnetic field environment over 0.1 T.

The MCP-PMT with independently biased design shows significantly improved tolerance to magnetic field strength. The performance of the investigated MCP-PMT was measured at various magnetic field strengths and bias high voltages. An external HV divider was used to ensure both MCPs were biased at the same HV for best performance. At a fixed magnetic field strength, the signal amplitude of the MCP photodetector increases as the bias high voltage increases. This behavior is similar to our previous measurements of the MCP-PMT without applying a magnetic field [21]. At a fixed bias voltage of 3100 V, the signal amplitude of the MCP-PMT increases slightly as the magnetic field strength increases to 0.2 T, and then decreases as the magnetic field strength continues to increase, and eventually breaks down with signal amplitude below 5 mV at magnetic field strength of 0.7 T. With lower biased voltages, the break down magnetic field strengths decrease accordingly. From these results, one may compensate the effect of magnetic field on the MCP-PMT gain by increasing the applied bias voltage, with lower HV at low magnetic field strength while higher HV at high magnetic field strength to maintain the same gain for MCP-PMT operation.

4.2. Tilt angle dependence

With a good performance in the magnetic field, MCP-PMT with the independently biased design was chosen to study its performance dependence on tilt angle between the normal to the MCP-PMT window and the direction of the magnetic field, as shown in Fig. 3. We applied a fixed high voltage of 3000 V on the HV divider and rotated the tilt angles θ from -90° to 90° for a full range angle measurement. Fig. 6 presents the response of the MCP-PMT, in terms of the signal amplitude, as a function of the tilt angle at two magnetic field strengths of 0.25 and 0.5 Tesla, respectively. The signal amplitude shows strong angle dependence at -30° $\leq \theta \leq$ 30° with two local maximums at 8°. The peak angles of 8° are due to the original 8° bias angle of the two MCPs and their chevron configuration. When the direction of one MCP pore is aligned with the direction of the magnetic field, the MCP-PMT shows an enhanced magnetic field tolerance. The signal maximum at 8° corresponds to the position where the direction of top MCP pore is aligned with the direction of the magnetic field, and the signal maximum at -8° corresponds to the position where the direction of bottom MCP pore is aligned with the direction of the magnetic field. The signal amplitude value at 8° is higher that of -8°, indicating that the effect from the direction of top MCP pores is stronger than that from the bottom MCP pores.

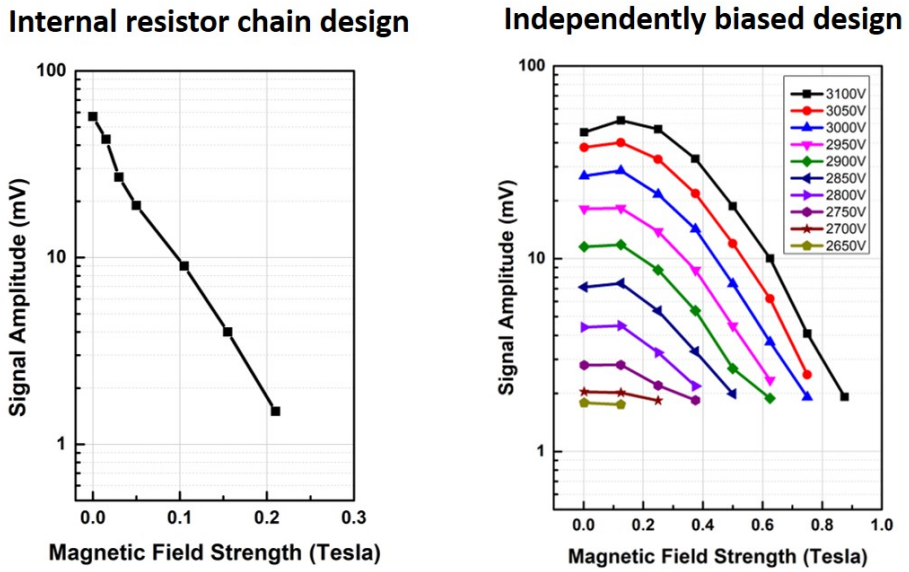

Figure 5: Performance of the MCP-PMTs in terms of signal amplitude in magnetic field: the internal resistor chain design (left) and the independently biased design (right). The magnetic field tolerance of MCP-PMT is significantly improved with bias voltages of both MCPs at optimized values.

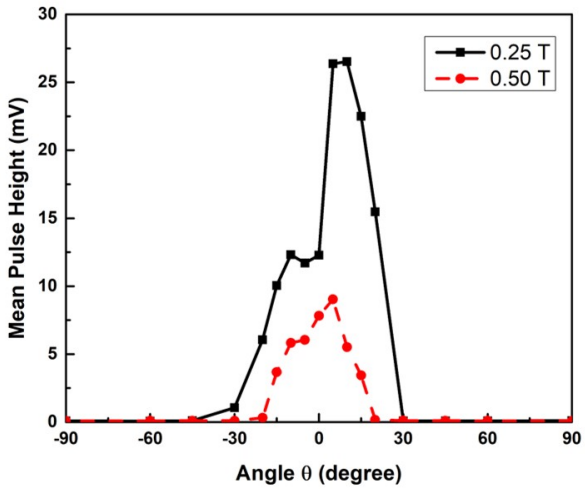

Figure 6: The response of the MCP-PMT as a function of the tilt angles θ between the normal to the MCP-PMT window and the direction of the magnetic field. The two peaks around -8° and 8° indicates the effect due to the 8° bias angle of the MCPs. Note that the intensities of these two peaks are not the same due to the different effect of the top and bottom MCPs.

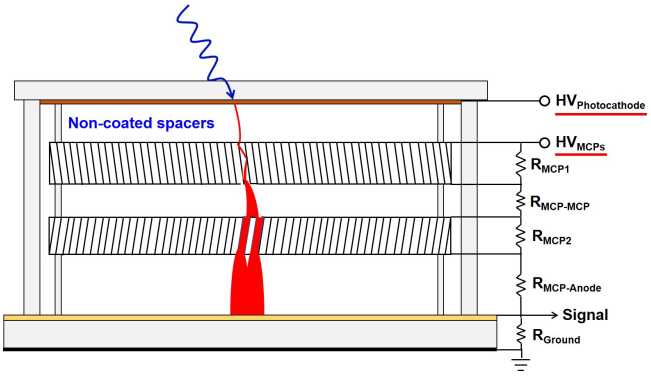

Figure 7: The electrical circuit of HV connections to vary the gap voltage between the photocathode and the top MCP.

4.3. Gap high voltage dependence

The MCP-PMT performance dependence on HV applied to the gap between the photocathode, and top MCP was also studied at different magnetic field strengths. Fig. 7 shows the circuit diagram to vary the applied gap voltage between the photocathode and top MCP during this measurement. The HV of the MCPs was kept at a fixed value, and the HVPhotocathode was varied at different values to adjust the applied gap voltage.

The pulsed signals were recorded, and the signal amplitudes were calculated and plotted as in Fig. 8. At the low magnetic field, the signal amplitude increases as the gap voltage increases and reaches a maximum at gap voltage 500 V, and then the signal amplitude starts to decrease with continuously increased gap voltage. The behavior of MCP-PMT signal amplitude dependence on the gap voltage at the low magnetic field is due to the effect of primary

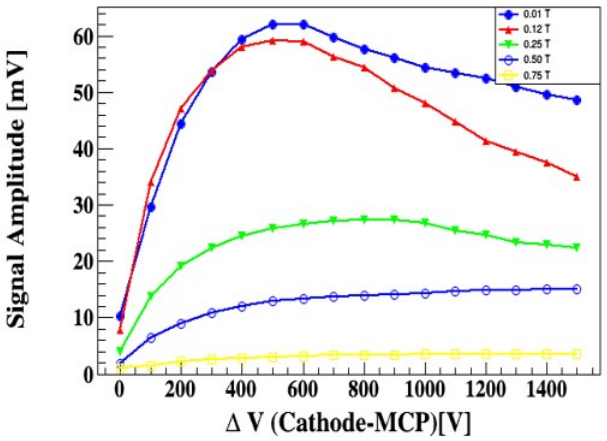

Figure 8: Performance of the MCP-PMTs in terms of signal amplitude as a function of gap voltage applied between the photocathode and top MCP in different magnetic fields.

electron energy on the secondary emission yield of ALD coated emissive materials. The MCPs used here were processed with ALD coated emissive materials for secondary emission with their secondary emission yields dependence on surface composition and film thickness studied previously [22]. The measurement data shows that the secondary emission yield of the ALD coated material has the highest value when the primary electron energy is around 300 eV 500 eV, resulting in the maximum signal amplitude for the investigated MCP-PMT with photocathode to MCP gap HV at 500 V. The secondary yield of the ALD coated material starts to decrease with even higher primary electron energy, leading to reduced signal amplitude at over 500 V gap voltage. At high magnetic fields, the magnetic field strength becomes the main parameter affecting the secondary emission process. The secondary yield of the ALD coated material does not decrease anymore with primary electron energy over 500 eV, resulting in a continuously increased signal amplitude even with higher gap voltages.

5. Conclusions

Two 6×6 cm^2 MCP-PMTs with internal resistor chain design and independently biased design were fabricated at Argonne National Laboratory and characterized with the Argonne magnetic field test facility. The behavior of the MCP-PMT signal amplitude was investigated as a function of the magnetic field strength, the distribution of bias voltage, the tilt angle and the gap voltage. It was found that the MCP-PMT with internal resistor chain design only shows magnetic field tolerance up to 0.1 T. With independently biased voltage design, the magnetic field tolerance of the MCP-PMT is significantly improved up to 0.7 T. It is essential to ensure both MCPs are operated at optimal bias voltage for applications in high magnetic fields. As the magnetic field strength increases, the signal amplitude of the MCP-PMT decreases for operation at the same bias voltage, the reduction of signal amplitude can be compensated by increasing the operation voltage, extending the MCP-PMT operation limit in the high magnetic field. Due to the original MCP bias angle of 8° and the chevron configuration, the MCP pores are not aligned with the direction of the magnetic field when the MCP-PMT window surface is normal to the direction of the magnetic field. The MCP-PMT shows higher signal amplitudes when either MCP pores are aligned with the direction of the magnetic field, and the direction alignment of the top MCP pores exhibits a stronger impact on the MCP-PMT performance than that of the bottom MCP pores. Increasing the bias voltage applied on the gap between the photocathode and the top MCP results in a maximum signal amplitude with gap voltage around 500 V at low magnetic fields, while a continuously increased signal amplitude at high magnetic fields.

6. Acknowledgments

The authors thank Frank Skrzecz (Engineer at ANL) for his mechanical engineering support; Joe Gregar (Scientific Glass Blower at ANL) for his talented work on glass parts; Mark Williams and Wilson Miller (Professors at University of Virginia) for their arrangement of the University of Virginia MRI magnet usage; Peter Winter (Physicist at ANL) for his arrangement of the Argonne 4-Tesla magnetic facility usage; and many people from the LAPPD collaboration for their advice and assistance. This material is based upon work supported by the U.S. Department of Energy, Office of Science, Office of High Energy Physics, Office of Nuclear Physics, under contract number DE-AC02-06CH11357. Work at Thomas Jefferson National Accelerator Facility was supported by the U. S. Department of Energy, Office of Science under contract No. DE-AC05-06OR23177. Work at Brookhaven National Laboratory was supported by the U. S. Department of Energy, Office of Science under contract No. DE-SC0012704. This work was also partially supported by the EIC R&D funding from the Office of Nuclear Physics and Office of Science of the U.S. Department of Energy.

References

[1] A. Accardi, et al., Electron ion collider: The next QCD frontier, Eur. Phys. J. A 52 (2016) 268.
[2] A. Aprahamian, et al., Reaching for the horizon: The 2015 long range plan for nuclear science (2015).
[3] A. Kiselev, BeAST Detector (Brookhaven eA Solenoidal Tracker), presentation on Electron Ion Collider User Group Meeting, Berkeley, CA (2016).
[4] PHENIX Collaboration, Concept for an Electron Ion Collider (EIC) detector built around the BaBar solenoid, arXiv:1402.1209.
[5] G. Wei, et al., Integration of the full-acceptance detector into the JLEIC, Proceedings of IPAC2017, THPAB084, Copenhagen, Denmark (2017).

[6] J. Repond, TOPSiDE Concept of an EIC Detector, Workshop on Streaming Readout, Boston, MA (2018).
[7] J. L. Wiza, Microchannel plate detectors, Nucl. Instr. and Meth. A 162 (1979) 587.
[8] B. Adams, et al., A brief technical history of the Large-Area Picosecond Photodetector (LAPPD) Collaboration, (2016) arXiv:1603.01843.
[9] M. Minot, et al., Pilot production & commercialization of LAPPD, Nucl. Instr. and Meth. A 787 (2015) 78.
[10] A. U. Mane, et al., An atomic layer deposition method to fabricate economical and robust large area microchannel plates for photodetectors, Physics Procedia, 37 (2012) 722.
[11] M. Popecki et al., Microchannel plate fabrication using glass capillary arrays with atomic layer deposition films for resistance and gain, J. Geophys. Res. Space Phys., 121 (2016) 7449.
[12] A. O'Mahony et al., Atomic layer deposition of alternative glass microchannel plates, J. Vac. Sci. Tech., 34 (2016) 01A128.
[13] T. M. Conneely, J. S. Milnes, and J. Howorth, Extended lifetime MCP-PMTs: Characterisation and lifetime measurements of ALD coated microchannel plates, in a sealed photomultiplier tube, Nucl. Instr. and Meth. A 732 (2013) 388.
[14] O. H. W. Siegmund, et al., Performance characteristics of atomic layer functionalized microchannel plates, Proc. SPIE 8859, (2013) 88590Y.
[15] J. Xie, et al., Development of a small form-factor (6 6 cm2) picosecond photodetector as a path towards the commercialization of large area devices, Proceeding of The Technology and Instrumentation in Particle Physics 2014, PoS (2014).
[16] Incom, Inc.: http://www.incomusa.com/
[17] B. Adams, et al., Measurements of the gain, time resolution, and spatial resolution of a 2020 cm2 MCP-based picosecond photo-detector, Nucl. Instr. and Meth. A 732 (2013) 392.
[18] 4 Tesla Magnet Facility: https://www.anl.gov/hep/group/4-tesla-magnet-facility
[19] DT5742 desktop digitizer: http://www.caen.it
[20] DRS chip developed at Paul Scherrer Institute, Switzerland: https://www.psi.ch/drs
[21] J. Wang et al., Development and testing of cost-effective, 6 cm 6 cm MCP-based photodetectors for fast timing applications, Nucl. Instr. and Meth. A 804 (2015) 84.
[22] S. Jokela et al., Secondary electron yield of emissive materials for large-area micro-channel plate detectors: surface composition and film thickness dependencies, Physics Procedia 37 (2012) 740.